Pergamon

Int. J. Solids Structures Vol. 33, No. 8, pp. 1069–1082, 1996

0020-7683/96 $15.00 + .00

0020-7683(95)00071-2

EFFECT OF ELASTICITY ON SLIP SYSTEM ACTIVITY IN FACE-CENTERED CUBIC CRYSTALS: A NUMERICAL STUDY

ANTOINETTE M. MANIATTY and JIUN-SHYA YU
Department of Mechanical Engineering, Aeronautical Engineering and Mechanics, Rensselaer Polytechnic Institute, Troy, NY 12180, U.S.A.

(*Received* 21 *October* 1994; *in revised form* 3 *March* 1995)

Abstract—The effect elasticity may play on the number of active slip systems in face-centered cubic (fcc) crystals in polycrystalline metals is investigated. In this work, an elastoviscoplastic polycrystalline model is used for the analysis. The deformation in each crystal is assumed to be composed of three parts, plastic slip along crystallographic slip systems, an elastic stretch of the lattice and a rigid rotation of the lattice. It is commonly believed that for metals at large strains, the elastic part of the deformation can be neglected in many cases. It has been shown that at least five slip systems must be active to accommodate any arbitrary plastic deformation. In this study, it is shown that, with the inclusion of elasticity, the model predicts that a significant number of grains have less than five active slip systems, even at large strains. In addition, it is also found that the number of active slip systems is significantly affected by the values of the elastic constants.

NOTATION

The following notational conventions are used in this paper. Vector quantities are expressed in lower case bold, for example $\mathbf{v}$, tensors in upper case bold, for example $\mathbf{A}$, and fourth order tensors in upper case bold script, for example $\mathscr{A}$. The product of two tensors is written as $\mathbf{AB}$, which is defined in components as $(\mathbf{AB})_{ik} \equiv A_{ij}B_{jk}$, where summation is implied on repeated indices. The inner product is always denoted by a dot ($\cdot$). For tensors, the inner product is defined as $\mathbf{A}\cdot\mathbf{B} \equiv \mathrm{tr}(\mathbf{A}^T\mathbf{B})$, where superscript T denotes the transpose and tr is the trace operator. A dyadic product is always denoted by the symbol ($\otimes$). for vectors the dyadic product is written as $\mathbf{u}\otimes\mathbf{v}$ and is defined in component form as $(\mathbf{u}\otimes\mathbf{v})_{ij} \equiv u_i v_j$. The operation of a fourth order tensor ($\mathscr{A}$) on a second order tensor ($\mathbf{B}$) is denoted as $\mathscr{A}[\mathbf{B}]$.

INTRODUCTION

Modeling metal polycrystals undergoing large deformations using microstructural phenomenology has been a topic of great interest for many years. Taylor and Elam (1923, 1925) proposed one of the earliest quantitative descriptions of plastic deformation in single crystals by observing that plastic deformation occurs along certain crystallographic slip systems when the resolved shear stress on these systems exceeds some critical value. Von Mises (1928) noted that five independent slip systems are needed for arbitrary, uniform, isochoric, plastic deformation in individual crystals of a polycrystalline aggregate. This is because the plastic rate of deformation tensor for a volume-preserving deformation is a traceless, symmetric, second-order tensor with five independent components. To accommodate the five independent components, five non-redundant slip systems in a single crystal are needed. Later, it was derived by Bishop and Hill (1951a, b) that there are 56 vertices on the yield surface in five-dimensional deviatoric stress space for a face-centered cubic (fcc) crystal. Furthermore, they found that the yield stresses corresponding to any applied deformation could be located at one of these vertices or on an "edge" between vertices, and the yield stresses can be determined from the Principle of Maximum Work. Kocks *et*

al. (1983) have tabulated these 56 vertices with corresponding active slip systems and the various edges between different vertices, and they show that there are either six or eight slip systems active at each vertex.

In addition to modeling the behavior of individual crystals, it is necessary to model the interaction between crystals in a polycrystalline aggregate. The simplest interaction law is that proposed by Taylor (1938), which assumes that every grain in a polycrystalline aggregate undergoes the same rate of deformation as the whole. Therefore, both local and global compatibility are satisfied, but equilibrium may be violated across grain boundaries. Taylor's model has been found to be a good approximation for single-phase, cubic, metal polycrystals with fine grain structures when the grains are fairly equi-axed (Kocks, 1970). Since each grain is assumed to experience uniform deformation equal to the global deformation, the models for the single crystals can be applied directly to each grain with appropriate kinematic constraints.

In these early works, the elastic part of the deformation (lattice stretching) was usually neglected, since the elastic part of the deformation is generally very small compared to the plastic part for polycrystalline metals undergoing large strains. Neglecting elasticity, it can be shown that the corners (vertices) of the yield surface represent stable stress states. For an fcc crystal, states of stress on the edges of the yield surface, which have four active slip systems, or on surfaces of the yield surface, which have less than four active slip systems, are unstable states that arise only if the rate of deformation tensor is precisely normal to an edge or surface. The probability of the rate of deformation tensor being precisely normal to an edge or surface is zero. Therefore, it is commonly assumed that for an fcc crystal in a polycrystalline aggregate, there are always six or eight active slip systems during plastic yielding, and the stress state for each crystal is in a corner of the yield surface.

A problem with these early models was that the shear rates could not be uniquely determined from the global stress. This is because the rate of deformation tensor is defined to be normal to the yield surface, but the normal is non-unique at a corner. This problem can be resolved by using a viscoplastic constitutive model. Pan and Rice (1983) illustrated that when a rate-dependent relationship is assumed between the resolved shear stress and the shear rate on a slip system, the vertices will become rounded and the shear rate values can be uniquely determined from the global stresses. The edges and surfaces of the flow surface (analogous to the yield surface in the rate-independent case) remain flat in the viscoplastic case. Therefore, the model still predicts that the stress state will always be in a corner, although now rounded, with six or eight active slip systems for an fcc crystal, and at least five active slip systems in general.

Although the viscoplastic theory of deformation in polycrystals based on crystallographic slip predicts that there are at least five active slip systems for an arbitrary deformation in each grain of a polycrystalline aggregate, experiments have shown otherwise in many cases. This is due to the assumptions in the model which may not be valid. For example, the model assumes a uniform deformation, both globally for the aggregate and locally within each grain. In polycrystals with many crystals on the surface of the specimen which are not constrained by adjacent crystals (particularly the case in coarse-grained polycrystals), the deformation in each crystal has been observed to be non-uniform with different slip systems active near grain boundaries than elsewhere (Fleischer and Chalmers, 1958; Fleischer and Backofen, 1960; Fleischer and Hosford, 1961). If the deformation is non-uniform, the requirement of at least five active slip systems is no longer necessary. Fleischer (1987) counted the number of active slip systems in deformed polycrystalline brass in grains fully constrained by neighboring crystals and found that approximately 40% of the grains had less than five active slip systems. This indicates that the deformation may be non-uniform, even in confined grains within a polycrystal. Another reason for less than five active slip systems is that other modes of deformation which are not included in the model, such as twinning, may accommodate part of the deformation and reduce the required number of slip systems. One such mode of deformation which is often considered negligible is the elastic stretch of the lattice.

In this paper, elasticity is included in the model for fcc material and the predicted effect on the number of active slip systems is investigated. It is found that when elasticity is

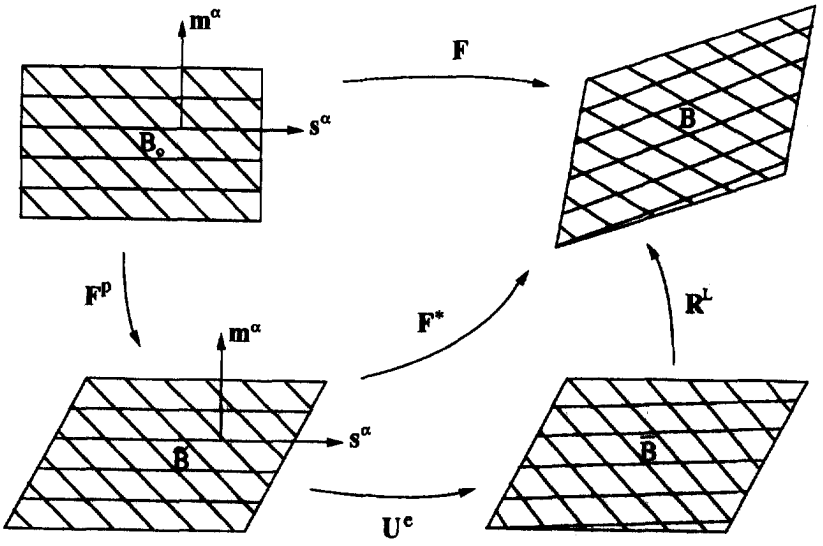

Fig. 1. Kinematics for a single crystal.

included in the model, the model predicts that a significant number of grains in the polycrystalline aggregate have less than five active slip systems, even at large deformations.

ELASTO-VISCOPLASTIC MODEL

In this work, it is assumed that the deformation of a ductile single crystal can be decomposed into a lattice rotation, an elastic stretch of the lattice and a plastic shearing along crystallographic slip planes, as shown schematically in Fig. 1. The structure of kinematics follows that given in Peirce *et al.* (1983). Summarizing, a multiplicative decomposition of the deformation gradient **F** into elastic (lattice) and plastic components as first proposed by Lee (1969) is used, giving

$$\mathbf{F} = \mathbf{F}^*\mathbf{F}^p \quad \det\mathbf{F}^p = 1 \quad \det\mathbf{F}^* > 0, \tag{1}$$

where $\mathbf{F}^*$ is the elastic (lattice) deformation gradient and $\mathbf{F}^p$ is the plastic deformation gradient. The plastic part of the deformation is assumed to be due to slip along crystallographic slip systems and is isochoric. The elastic part of the deformation, $\mathbf{F}^*$, can be further decomposed using the polar decomposition theorem to give

$$\mathbf{F}^* = \mathbf{R}^L\mathbf{U}^e \quad \mathbf{U}^{e^T} = \mathbf{U}^e, \tag{2}$$

where $\mathbf{R}^L$ is a rigid rotation of the lattice and $\mathbf{U}^e$ is the stretch of the lattice. Using eqn (1), the velocity gradient may be expressed as

$$\mathbf{L} = \dot{\mathbf{F}}\mathbf{F}^{-1} = \dot{\mathbf{F}}^*\mathbf{F}^{*-1} + \mathbf{F}^*\dot{\mathbf{F}}^p\mathbf{F}^{p-1}\mathbf{F}^{*-1}. \tag{3}$$

Furthermore, the velocity gradient can be decomposed into symmetric and anti-symmetric parts as

$$\mathbf{L} = \mathbf{D} + \boldsymbol{\Omega}, \tag{4}$$

where **D** is the symmetric rate of deformation tensor and $\boldsymbol{\Omega}$ is the spin tensor, the anti-symmetric part of **L**. Let

$$\mathbf{D} = \mathbf{D}^* + \mathbf{D}^p \quad \text{and} \quad \Omega = \Omega^* + \Omega^p, \tag{5}$$

where

$$\mathbf{D}^p + \Omega^p = \mathbf{F}^* \dot{\mathbf{F}}^p \mathbf{F}^{p^{-1}} \mathbf{F}^{*-1} \tag{6}$$

and where $\mathbf{D}^p$ and Ω^p are respectively the symmetric and anti-symmetric parts of the plastic velocity gradient pushed forward by $\mathbf{F}^*$ to the current configuration B. Relating this to the plastic shearing on the cystallographic slip systems gives

$$\tilde{\mathbf{L}}^p = \dot{\mathbf{F}}^p \mathbf{F}^{p^{-1}} = \sum_{\alpha=1}^{N_s} \dot{\gamma}^\alpha \mathbf{P}^\alpha \quad \mathbf{P}^\alpha \equiv \mathbf{s}^\alpha \otimes \mathbf{m}^\alpha, \tag{7}$$

where $\tilde{\mathbf{L}}^p$ is the plastic velocity gradient expressed in the relaxed configuration $\tilde{B}$, $\dot{\gamma}^\alpha$ is the shear rate of slipping on the α slip system, $\mathbf{P}^\alpha$ is the Schmid tensor for the α slip system and N_s is the total number of slip systems. Furthermore, $\mathbf{s}^\alpha$ is a unit vector in the α slip direction and $\mathbf{m}^\alpha$ is a unit vector normal to the α slip plane. Finally, the resolved shear stress on the α slip system can be determined from

$$\tau^\alpha = \tilde{\mathbf{T}} \cdot (\mathbf{F}^* \mathbf{P}^\alpha \mathbf{F}^{*-1}) = (\mathbf{C}^e \tilde{\mathbf{T}}) \cdot \mathbf{P}^\alpha, \tag{8}$$

where $\tilde{\mathbf{T}}$ is the Kirchhoff stress, $\mathbf{C}^e \equiv \mathbf{F}^{*T} \mathbf{F}^* = \mathbf{U}^{e^2}$ is the right elastic Cauchy–Green tensor and $\tilde{\mathbf{T}}$ is the second Piola–Kirchhoff stress on the relaxed configuration $\tilde{B}$.

In addition to the kinematics specified above, a constitutive law is needed to relate the stress to the deformation. In this work, a power law is used to model the viscoplastic part of the constitutive law which relates the plastic shear stress τ^α to the shear rate $\dot{\gamma}^\alpha$ on the α slip system as follows:

$$\dot{\gamma}^\alpha = f(\tau^\alpha, g) = \dot{a} \left(\frac{\tau^\alpha}{g} \right) \left| \frac{\tau^\alpha}{g} \right|^{(1/m)-1}, \tag{9}$$

where g is an internal variable which represents the resistance to flow on all of the slip systems in the grain, $\dot{a}$ is a reference shear rate and m is the material rate sensitivity. An evolution equation for the internal variable g is also needed. The relation taken here is that given by Kocks (1976) and can be summarized as follows:

$$\dot{g} = h(\dot{\gamma}, g) \dot{\gamma} \tag{10}$$

$$\dot{\gamma} \equiv \sum_{\alpha=1}^{N_s} |\dot{\gamma}^\alpha| \tag{11}$$

$$h(\dot{\gamma}, g) = \Theta_0 \left(\frac{\tau_s(\dot{\gamma}) - g}{\tau_s(\dot{\gamma}) - \tau_0} \right) \tag{12}$$

$$\tau_s(\dot{\gamma}) = \tau_{s_0} \left| \frac{\dot{\gamma}}{\dot{\gamma}_0} \right|^{A/\mu} \tag{13}$$

where μ is the elastic shear modulus and Θ_0, τ_0, τ_{s_0}, $\dot{\gamma}_0$ and A are material parameters.

The elastic constitutive behavior must also be specified. An anisotropic linear relationship with cubic symmetry is used. It can be expressed as

$$\tilde{\mathbf{T}} = \mathscr{L}[\mathbf{E}^e] = 2\mu\mathbf{E}^e + \lambda(\operatorname{tr}\mathbf{E}^e)\mathbf{I} - 2\beta\mathscr{C}[\mathbf{E}^e], \quad \mathbf{E}^e = \tfrac{1}{2}(\mathbf{C}^e - \mathbf{I}), \tag{14}$$

where $\mathscr{L}$ is the fourth order elasticity tensor, μ, λ and β are the elastic constants, $\mathbf{E}^e$ is the elastic Green strain which is work conjugate with the second Piola–Kirchhoff stress, $\tilde{\mathbf{T}}$ and $\mathscr{C}$ is a fourth order tensor defined by the symmetries of the cube and its orientation. In the lattice coordinates, the components of the fourth order tensor $\mathscr{C}$ are defined as follows:

$$\mathscr{C}_{ijkl} = \begin{cases} 1 & \text{if } i = j = k = l \\ 0 & \text{otherwise.} \end{cases}$$

It is clear that when $\beta = 0$, the elastic relationship is isotropic, therefore β represents the degree of anisotropy. In terms of the three independent components of the fourth order elasticity tensor $\mathscr{L}$ in the lattice coordinates,

$$\beta = \tfrac{1}{2}(2\mathscr{L}_{1212} + \mathscr{L}_{1122} - \mathscr{L}_{1111}).$$

The Cauchy stress $\mathbf{T}$ can then be derived from $\tilde{\mathbf{T}}$ and $\mathbf{F}^*$ as

$$\mathbf{T} = \frac{1}{\det \mathbf{F}^*}\mathbf{F}^*\tilde{\mathbf{T}}\mathbf{F}^{*T}. \tag{15}$$

Equations (1)–(15) completely define the behavior of the individual grains in a polycrystalline aggregate. These equations are integrated using the algorithm given in Maniatty *et al.* (1992). A summary of the algorithm is given here in Appendix A. The Taylor assumption is used for modeling the grain interaction, i.e. the global deformation is applied to each grain of a polycrystalline aggregate.

ELASTIC EFFECTS

Although the elastic deformation is in general very small relative to the plastic deformation during large strains, it may have a surprisingly large effect on the slip system activity. Consider a purely viscoplastic analysis for comparison. Since the elastic stretch of the lattice is relatively small, it seems reasonable to make the following approximations:

$$\mathbf{U}^e \approx \mathbf{I} \quad \mathbf{F}^* \approx \mathbf{R}^L, \tag{16}$$

where $\mathbf{I}$ is the identity tensor. This is what is assumed in a purely viscoplastic analysis. If this approximation is substituted into eqn (3) for the velocity gradient, one obtains

$$\mathbf{L} = \dot{\mathbf{R}}^L\mathbf{R}^{L^T} + \mathbf{R}^L\tilde{\mathbf{L}}^P\mathbf{R}^{L^T}, \tag{17}$$

where $\dot{\mathbf{R}}^L\mathbf{R}^{L^T} = \Omega^L$ is an anti-symmetric tensor representing the lattice spin. Decomposing the velocity gradient into symmetric and anti-symmetric components gives

$$\mathbf{D} = \mathbf{R}^L\tilde{\mathbf{D}}^P\mathbf{R}^{L^T} = \mathbf{D}^P \quad \tilde{\mathbf{D}}^P \equiv \tfrac{1}{2}(\tilde{\mathbf{L}}^P + \tilde{\mathbf{L}}^{P^T}) \tag{18}$$

$$\Omega = \Omega^L + \mathbf{R}^L\tilde{\Omega}^P\mathbf{R}^{L^T} = \Omega^L + \Omega^P \quad \tilde{\Omega}^P \equiv \tfrac{1}{2}(\tilde{\mathbf{L}}^P - \tilde{\mathbf{L}}^{P^T}). \tag{19}$$

Comparing the above equations with those in eqn (5), one can see that the primary difference is that in the viscoplastic case the global rate of deformation is equal to the plasic rate of deformation, while in the elasto-viscoplastic case there is also an elastic contribution, $\mathbf{D}^*$. This means that in the viscoplastic case the total rate of deformation $\mathbf{D}$ is solely accommodated by crystallographic slip, whereas in the elasto-viscoplastic case part of the rate of

Table 1. Parameters for the Voce–Kocks model for 1100 aluminum.

$\dot{a} = 1\ \text{s}^{-1}$	$\tau_{s_0} = 61.82$ MPa
$m = 0.05$	$\dot{\gamma}_0 = 5 \times 10^{10}\ \text{s}^{-1}$
$g_0 = 27.17$ MPa	$\mu = 25.3$ GPa
$\tau_0 = 27.17$ MPa	$\lambda = 54.4$ GPa
$\Theta_0 = 56.41$ MPa	$\beta = 4.54$ GPa
$A = 0.129$ GPa	

deformation can be accommodated by the elastic stretching of the lattice. This eliminates the requirement of five active slip systems for an arbitrary deformation because the elastic part of the deformation can theoretically always accommodate what the plastic part does not.

One may expect, however, that the elastic effects are only transient and become negligible at large strains. An argument for this is that for a constant rate of deformation, the stress reaches a near constant value (saturates) at finite strains, and therefore the elastic strain will be near constant since it is linearly related to the stress. If the elastic strain is nearly constant, then the elastic rate of deformation, $\mathbf{D}^*$, will become nearly zero. This is true at the macroscopic level; however, at the micromechanical level, one must remember that the grains will continue to reorientate throughout the deformation up to very large strain levels. Therefore, at the micromechanical level, a steady-state is not achieved. In fact, the stress state in an individual grain of a polycrystal will move from one vertex to another on the flow surface as the grain continues to rotate. In the viscoplastic model the stress state in a grain will "jump" from one vertex to another, but in the elasto-viscoplastic model the stress state will move more gradually from one vertex to another. The effect of this is that, even at large deformations, the elasto-viscoplastic model always predicts that some grains in the polycrystal will have stress states between vertices, on an edge or surface, in a state with less than five active slip systems. Numerical examples that demonstrate this are given in the next section.

Although the inclusion of elasticity affects the slip system activity and stress state at the microstructural level, it has virtually no effect on the texture evolution. This is shown in Maniatty *et al.* (1992), who compare an elasto-viscoplastic analysis with a viscoplastic analysis. They demonstrate that elasticity has no noticeable effect on the texture evolution or on the global deviatoric stresses that result under steady loading conditins. However, elasticity can affect the global stresses in cases of reverse loadings and in other non-steady conditions.

NUMERICAL EXAMPLES

In the following examples, the material is taken to be 1100 aluminum, an fcc material, with the material parameters as listed in Table 1. Table 2 lists the slip plane normals $\mathbf{m}^\alpha$ and the slip directions $\mathbf{s}^\alpha$ for each of the 12 primary slip systems for an fcc crystal.

Example 1

Consider a crystal in the cube orientation, i.e. with $\mathbf{R}^L = \mathbf{I}$, subjected to the following velocity gradient $\mathbf{L}$:

$$\mathbf{L} = \begin{bmatrix} a & b & 0 \\ b & -a & 0 \\ 0 & 0 & 0 \end{bmatrix} \quad \text{and} \quad a^2 + b^2 = 0.0001,$$

where the parameter a can take on values ranging from -0.01 to 0.01. Since the only components of the deviatoric stress tensor with non-zero values are T'_{11}, T'_{22} and T'_{12}, the constant plastic work flow surface can be plotted conveniently in two dimensions. Furthermore, due to the symmetry of the cube, only the upper right quadrant of the flow

Table 2. Slip systems for an fcc crystal

Slip system number	Slip plane normal, $\mathbf{m}^\alpha$	Slip direction, $\mathbf{S}^\alpha$
1	$1/\sqrt{3}, 1/\sqrt{3}, 1/\sqrt{3}$	$0, 1/\sqrt{2}, -1/\sqrt{2}$
2	$1/\sqrt{3}, 1/\sqrt{3}, 1/\sqrt{3}$	$-1/\sqrt{2}, 0, 1/\sqrt{2}$
3	$1/\sqrt{3}, 1/\sqrt{3}, 1/\sqrt{3}$	$1/\sqrt{2}, -1/\sqrt{2}, 0$
4	$-1/\sqrt{3}, -1/\sqrt{3}, 1/\sqrt{3}$	$0, -1/\sqrt{2}, -1/\sqrt{2}$
5	$-1/\sqrt{3}, -1/\sqrt{3}, 1/\sqrt{3}$	$1/\sqrt{2}, 0, 1/\sqrt{2}$
6	$-1/\sqrt{3}, -1/\sqrt{3}, 1/\sqrt{3}$	$-1/\sqrt{2}, 1/\sqrt{2}, 0$
7	$-1/\sqrt{3}, 1/\sqrt{3}, 1/\sqrt{3}$	$0, 1/\sqrt{2}, -1/\sqrt{2}$
8	$-1/\sqrt{3}, 1/\sqrt{3}, 1/\sqrt{3}$	$1/\sqrt{2}, 0, 1/\sqrt{2}$
9	$-1/\sqrt{3}, 1/\sqrt{3}, 1/\sqrt{3}$	$-1/\sqrt{2}, -1/\sqrt{2}, 0$
10	$1/\sqrt{3}, -1/\sqrt{3}, 1/\sqrt{3}$	$0, -1/\sqrt{2}, -1/\sqrt{2}$
11	$1/\sqrt{3}, -1/\sqrt{3}, 1/\sqrt{3}$	$-1/\sqrt{2}, 0, 1/\sqrt{2}$
12	$1/\sqrt{3}, -1/\sqrt{3}, 1/\sqrt{3}$	$1/\sqrt{2}, 1/\sqrt{2}, 0$

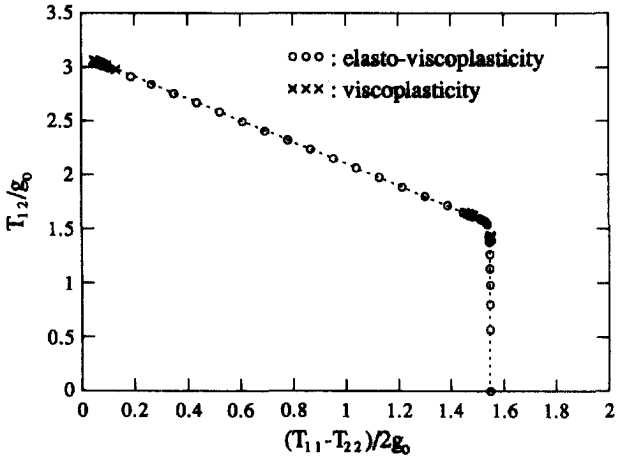

Fig. 2. Flow surface for constant plastic work = $0.2\,g_0$ comparing results from the elasto-viscoplastic model with the viscoplastic model.

surface needs to be plotted. The flow surface in this example is taken to be the stress surface for which the plastic work equals a constant. The plastic work is computed from

$$W^{\mathrm{p}} = \int_0^t \mathbf{T}' \cdot \mathbf{D}^{\mathrm{p}}\, \mathrm{d}t',$$

where $\mathbf{T}'$ is the deviatoric stress tensor. Constant plastic work flow surfaces for plastic work equal to $0.2\,g_0$ per unit volume are plotted in Fig. 2. The dotted line in the figure indicates the rate-independent yield surface predicted by the Principle of Maximum Work, which neglects elasticity. Two corners appear in the quadrant of the flow surface shown. For all sample values of a, the Principle of Maximum Work predicts that the yield stress will be in one of the corners. The crosses indicate the resulting stresses from the viscoplastic analysis. The stress state is still always in a corner, but now the corners are rounded. The open circles indicate the resulting stresses from the elasto-viscoplastic analysis, using the same sample values for a as used in the viscoplastic analysis. When the elastic effect is considered, the stress is either on an edge or in a corner.

Figure 3 shows flow surfaces for different levels of plastic work as predicted by an elasto-viscoplastic analysis. As the plastic work increases (along with the strain), the stresses become less likely to be on an edge and more likely to be in a corner. However, even at larger values of plastic work, there are still a significant number of cases where the stress is on an edge with only four slip systems active.

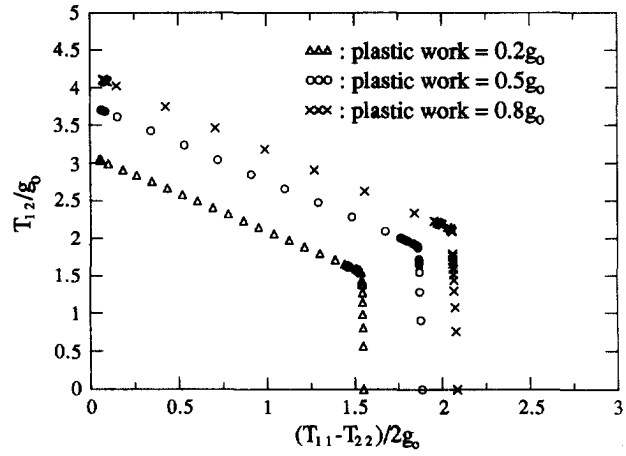

Fig. 3. Flow surfaces corresponding to different levels of plastic work.

Example 2

This example demonstrates the effect of the elastic stiffness on the slip system activity in a single crystal. Consider a crystal in the following orientaton, which was chosen at random:

$$\mathbf{R}^{\mathrm{L}} = \begin{bmatrix} -0.2873 & -0.4367 & -0.8525 \\ 0.6351 & 0.5794 & -0.5108 \\ 0.7170 & -0.6882 & 0.1109 \end{bmatrix}$$

subject to the velocity gradient

$$\mathbf{L} = \begin{bmatrix} 0.01 & 0 & 0 \\ 0 & -0.01 & 0 \\ 0 & 0 & 0 \end{bmatrix}.$$

Simulations were done for the case with the elastic parameters being the correct values as listed in Table 1 and for the cases with the elastic parameters being 10 times the actual values and 0.1 times the actual values. When the elastic parameters are 10 times the actual values, the elastic deformation will be much less than the actual elastic deformation, and the solution will be closer to the purely viscoplastic solution. When the elastic parameters are 0.1 times the actual values, the elastic part of the deformation will be larger than in reality and the effect of the elasticity will become more prominent.

For each case, a simulation was performed for 51 s. Figure 4 gives the evolution of the number of active slip systems with respect to effective strain, where the effective strain is defined as

$$\varepsilon_{\mathrm{eff}} = \int_0^t \sqrt{\tfrac{2}{3}\mathbf{D}\cdot\mathbf{D}}\,\mathrm{d}t'.$$

The shear rates on each of the slip systems at $t = 6$, 21, 36 and 51 s are shown in Table 3 for each of the three cases. Referring first to Fig. 4, the open circles represent the results from the case with elastic constants as the true values. At the beginning of deformation, the stress state stays on the edge, call it edge I, with only four active slip systems due to the small deformation. Then, as the deformation becomes larger, this state reaches one vertex, call it vertex A, with six active slip systems. When the grain deforms further, it reorientates and the stress state moves along another edge, call it edge J, with four active slip systems to another vertex, call it vertex B, with eight active slip systems. The crosses show the results

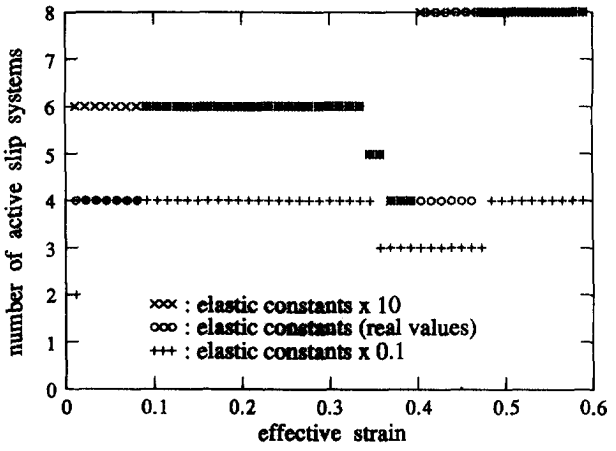

Fig. 4. Evolution of the number of active slip systems as a function of effective strain for different elastic constants.

Table 3. Rate of shear ($\dot{\gamma}^\alpha$, in s^{-1}) on the primary slip systems for example 3 with various elastic parameters

Slip system	$\dot{\gamma}^\alpha$ at $t = 6$ s	$\dot{\gamma}^\alpha$ at $t = 21$ s	$\dot{\gamma}^\alpha$ at $t = 36$ s	$\dot{\gamma}^\alpha$ at $t = 51$ s
For $\mu = 253$ GPa, $\lambda = 544$ GPa, $\beta = 45.4$ GPa				
1	0	0	0	0
2	0	0	0.000124	0.001399
3	0	0	0.000047	0.000159
4	−0.000070	−0.000058	0	0
5	0	0	−0.000618	−0.001410
6	−0.012337	−0.013237	−0.014700	−0.016700
7	0	0	0	0
8	0.000204	0.000363	0.001220	0.001990
9	0.012670	0.013951	0.014729	0.014126
10	−0.002964	−0.001380	0	0
11	−0.008130	−0.007723	−0.005857	−0.002006
12	0	0	−0.000047	−0.000190
For $\mu = 25.3$ GPa, $\lambda = 54.4$ GPa, $\beta = 4.54$ GPa				
1	0	0	0	0
2	0	0	0	0.001454
3	0	0	0	0.000162
4	0	−0.000053	0	0
5	0	0	0	−0.001421
6	−0.012298	−0.013212	−0.014965	−0.016755
7	0	0	0	0
8	0	0.000349	0.000931	0.002020
9	0.012778	0.013966	0.014926	0.014028
10	−0.002799	−0.001310	0	0
11	−0.008130	−0.007731	−0.005962	−0.001974
12	0	0	0	−0.000196
For $\mu = 2.53$ GPa, $\lambda = 5.44$ GPa, $\beta = 0.454$ GPa				
1	0	0	0	0
2	0	0	0	0
3	0	0	0	0
4	0	0	0	0
5	0	0	0	0
6	−0.011519	−0.012826	−0.015162	−0.018333
7	0	0	0	0
8	0	0	0	0.001907
9	0.012040	0.014002	0.015247	0.014607
10	−0.002589	−0.000881	0	0
11	−0.007998	−0.007842	−0.005513	−0.000951
12	0	0	0	0

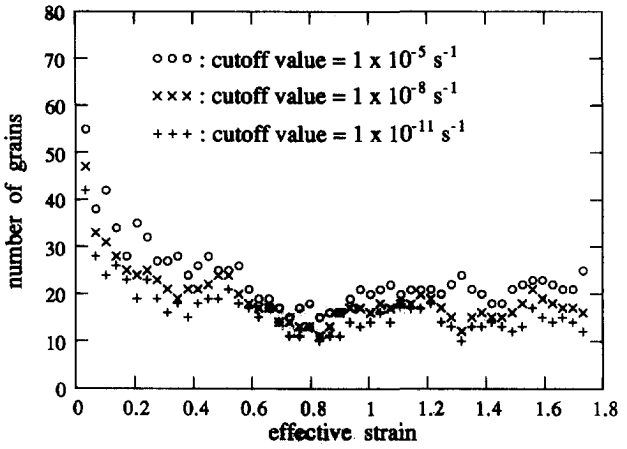

Fig. 5. Number of grains with less than five active slip systems in an aggregate composed of 200 randomly orientated grains. Three different cut-off values, $\dot{\gamma}_{\text{cut-off}}$, are used to judge whether each slip system is active or not.

for the case with the elastic constants 10 times the actual values. Because the elastic part of the deformation is very small in this case, the stress state is located on vertex A initially. Then, the grain rotates and the state moves to vertex B in a similar way as in the previous case, but with the stress state residing on edge J for a smaller time interval. Finally, the plus symbols represent the results from the case with elastic constants 0.1 times the true values. Since the elastic deformation is significant, the stress state stays on edge I for a longer time. Referring also to Table 3 now, it can be seen that, for the last case, before the stress state reaches vertex A, the stress state moves from edge I to edge J by crossing the surface between them. There are only three active slip systems on this surface. Then the stress state starts to approach vertex B. Because of the greater influence of the elastic deformation, the stress state does not reach any vertex during the first 51 s for this case.

Example 3

In this example, an aggregate composed of 200 initially randomly oriented grains under plane strain compression is analysed. The velocity gradient **L** applied to each grain is

$$\mathbf{L} = \begin{bmatrix} 0.01 & 0 & 0 \\ 0 & -0.01 & 0 \\ 0 & 0 & 0 \end{bmatrix}.$$

Figure 5 gives the number of grains with less than five active slip systems at different levels of effective strain. A criterion is required to judge whether a slip system is active or not, since the shear rate on each of the slip systems will never be exactly zero, but may be significantly less than on the "active" slip systems. Three different cut-off values for shear rate $\dot{\gamma}_{\text{cut-off}}$ are used in Fig. 5. When the effective strain is very small, there are a high percentage of grains that deform with only three or four slip systems because of strong elastic effects at the beginning of the process. However, even at large strains, with $\dot{\gamma}_{\text{cut-off}} = 1 \times 10^{-5}\ \text{s}^{-1}$, about 10% of the grains still deform with less than five slip systems.

To compare the effect of the elastic constants on the number of grains with less than five active slip systems, the aggregate was analysed with different values of elastic moduli with the same velocity gradient as above. The results are shown in Fig. 6, where $\dot{\gamma}_{\text{cut-off}} = 1 \times 10^{-5}\ \text{s}^{-1}$. As the elastic constants are increased, the elasto-viscoplastic analysis approaches the purely viscoplastic analysis, where all the grains have at least five active slip systems. As the elastic constants are decreased, a larger part of the deformation becomes elastic, and more of the grains have less than five active slip systems.

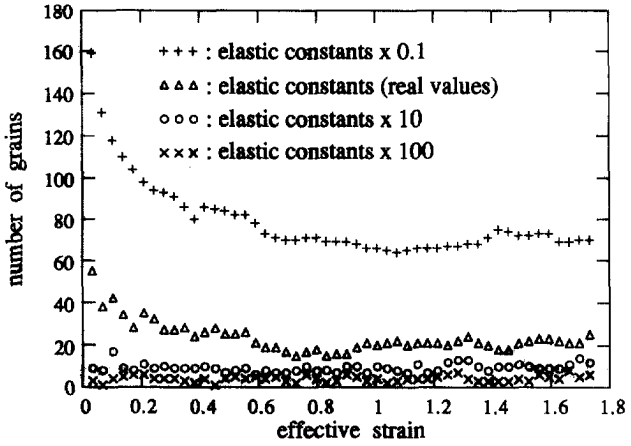

Fig. 6. Number of grains with less than five active slip systems in an aggregate composed of 200 randomly orientated grains. Four cases are analysed with different elastic constants and $\dot{\gamma}_{cut\text{-}off} = 1 \times 10^{-5}\ s^{-1}$ is taken as the cut-off value.

Table 4. Miller indices for the ideal orientations of four special textures

Texture	Miller indices
Brass	$\{110\}\langle 1\bar{1}2\rangle$
Copper	$\{112\}\langle 11\bar{1}\rangle$
Cube	$\{100\}\langle 001\rangle$
Goss	$\{110\}\langle 001\rangle$

Example 4

Here, the effect of the initial texture is considered. Four different initial textures are studied: brass, copper, cube and goss textures, which are often observed in experiments. The brass and copper textures usually result from large deformation processes, and the cube and goss textures are formed after recrystallization processes.

The Miller indices of the ideal orientations of these textures are listed in Table 4. These textures are generated by assuming that the grain orientations are rotationally symmetric Gaussian distributed about the ideal component, which can be expressed as

$$g(\omega) = g(0) \exp\left(-\frac{\omega^2}{2\omega_0^2}\right),$$

where $g(0)$ is the density of the ideal orientation, ω_0 is the scatter width of the spread and $g(\omega)$ is the relative density of a given orientation rotated through an angle ω from the ideal orientation. Following the procedure adopted by Lequeu *et al.* (1987), 200 grains are used to simulate these initial textures and the $\langle 111\rangle$ pole figures of these textures are shown in Fig. 7 with $\omega_0 = 15°$.

The following velocity gradient is applied to every grain in each initial texture:

$$\mathbf{L} = \begin{bmatrix} 0.01 & 0 & 0 \\ 0 & -0.01 & 0 \\ 0 & 0 & 0 \end{bmatrix}.$$

Figure 8 gives the number of grains with less than five active slip systems for each initial texture, where $\dot{\gamma}_{cut\text{-}off} = 1 \times 10^{-5}\ s^{-1}$.

For brass and copper textures, about 20% of the grains have less than five active slip systems at large strains. On the other hand, there are few grains with less than five active

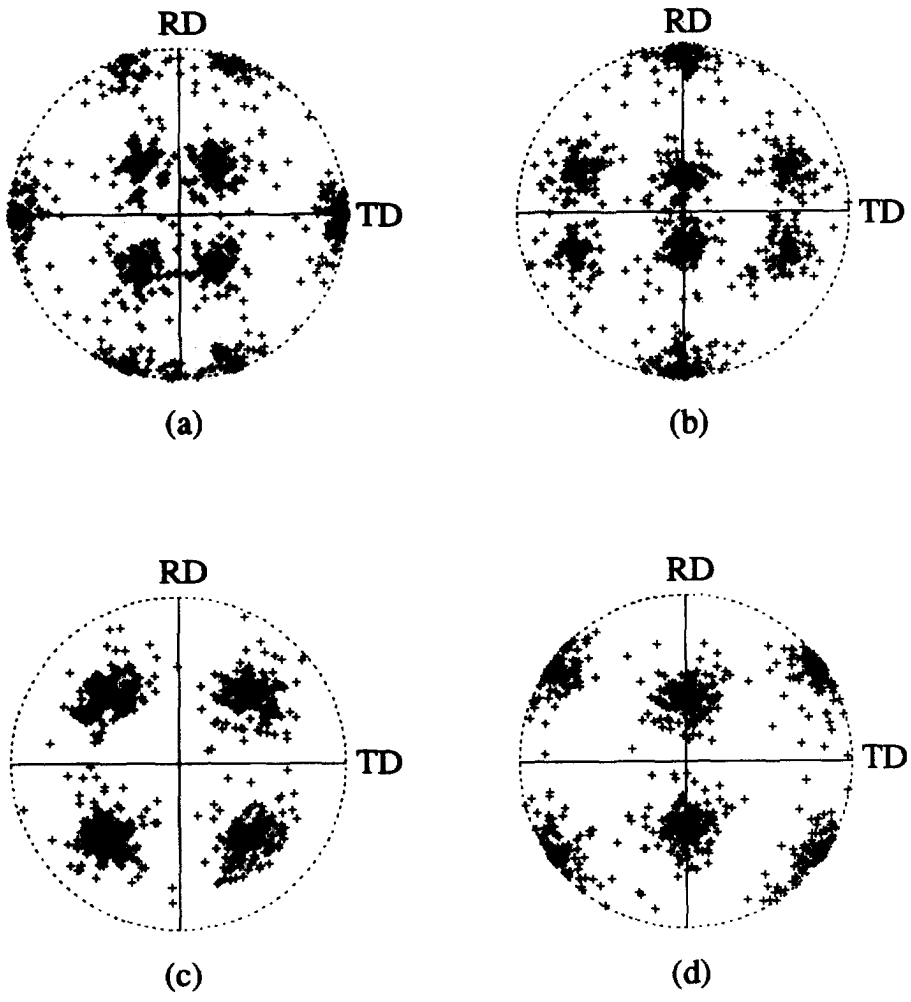

Fig. 7. ⟨111⟩ pole figures for initial textures modeled with 200 grains assuming rotationally symmetric Gaussian distributions with $\omega_0 = 15°$. The textures are as follows: (a) brass; (b) copper; (c) cube; (d) goss.

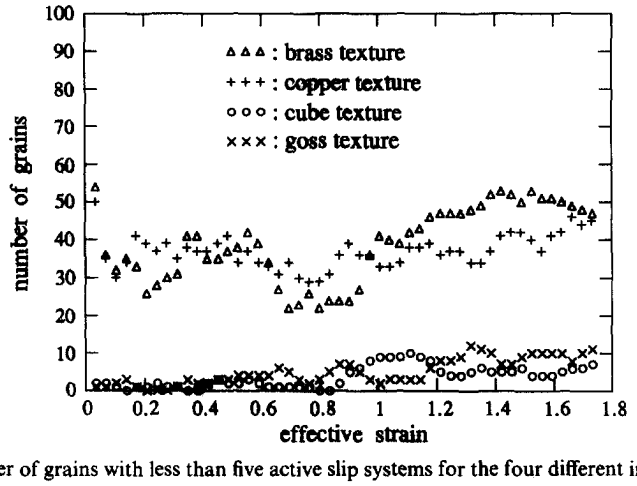

Fig. 8. Number of grains with less than five active slip systems for the four different initial textures.

slip systems for cube and goss textures. This is due to the fact that for the cube and goss texture, the grains are not reorientating much for this deformation, so the stress states in the grains stay in the vertices. However, for the brass and copper textures, the grains

continue to reorientate as the deformation progresses, so the stress states move in and out of the vertices on the flow surfaces.

CONCLUSIONS

Elasticity can have a noticeable effect on the slip system activity and the stress state in individual crystals of a polycrystal. It has been shown that when elasticity is included in the model for crystal deformation, a significant number of grains are predicted to have fewer than five active slip systems. When this occurs, the stress state is on an edge or a surface of the flow surface for fcc crystals. Furthermore, the magnitude of the elastic constants has an effect on the number of grains in a polycrystal with less than five active slip systems. Reducing elastic stiffness increases the number of grains with less than five active slip systems. While in reality it is not possible to reduce or increase a material's elastic stiffness, these results are interesting from a theoretical point of view, as they isolate the elastic effects from other effects. Also from these results, one would expect that a material with lower elastic constants and a higher resistance to plastic flow would experience the elastic effects observed herein more strongly.

Since whether or not the stress state stays in a vertex is dependent on the relationship between the grain orientation and the applied deformation rate, the initial texture plays an important role in the slip system activity. As shown in this paper, when the initial texture is a brass or copper texture, about 20% of the grains have less than five active slip systems under plane strain conditions; however, for a cube or goss texture, there are only a few grains with less than five active slip systems. This is because the cube and goss textures are stable, i.e. the grains do not reorientate much, under the plane strain conditions applied.

Acknowledgements—The authors are pleased to thank Professor D. Knorr for his thoughtful comments as this work was in progress. This work was supported by the Henry Luce Foundation, Inc. and by the National Science Foundation through Grant DMI-9358123.

REFERENCES

Bishop, J. F. W. and Hill, R. (1951a). A theory of the plastic distortion of a polycrystalline aggregate under combined stresses. *Phil. Mag.* **42,** 414–427.

Bishop, J. F. W. and Hill, R. (1951b). A theoretical derivation of the plastic properties of a polycrystalline face-centered metal. *Phil. Mag.* **42,** 1298–1307.

Fleischer, R. L. (1987). Number of active slip systems in polycrystalline brass: implications for ductility in other structures. *Acta Metall.* **35,** 2129–2136.

Fleischer, R. L. and Backofen, W. A. (1960). Effects of grain boundaries in tensile deformation at low temperatures. *Trans. Am. Inst. Min. Engrs* **218,** 243–251.

Fleischer, R. L. and Chalmers, B. (1958). Size effects in the deformation of aluminum. *Trans. Am. Inst. Min. Engrs* **212,** 265–274.

Fleischer, R. L. and Hosford, W. F. Jr (1961). Easy glide and grain boundary effects in polycrystalline aluminum. *Trans. Am. Inst. Min. Engrs* **221,** 244–247.

Kocks, U. F. (1970). The relation between polycrystal deformation and single-crystal deformation. *Metall. Trans.* **1,** 1121–1143.

Kocks, U. F. (1976). Laws for work-hardening and low-temperature creep. *J. Engng Mater. Technol.* **98,** 76–85.

Kocks, U. F., Canova, G. R. and Jonas, J. J. (1983). Yield vectors in fcc crystals. *Acta Metall.* **31,** 1243–1252.

Lee, E. H. (1969). Elastic–plastic deformation at finite strain. *J. Appl. Mech.* **36,** 1–6.

Lequeu, P. H., Gilormini, P., Montheillet, F., Bacroix, B. and Jonas, J. J. (1987). Yield surfaces for textured polycrystals—I. Crystallographic approach. *Acta Metall.* **35,** 439–451.

Maniatty, A. M., Dawson, P. R. and Lee, Y.-S. (1992). A time integration algorithm for elasto-viscoplastic cubic crystals applied to modeling polycrystalline deformation. *Int. J. Numer. Meth. Engng* **35,** 1565–1588.

Pan, J. and Rice, J. R. (1983). Rate sensitivity of plastic flow and implications for yield-surface vertices. *Int. J. Solids Structures* **19,** 973–987.

Peirce, D., Asaro, R. J. and Needleman, A. (1983). Material rate dependence and localized deformation in crystalline solids. *Acta Metall.* **31,** 1951–1976.

Taylor, G. I. (1938). Plastic strains in metals. *J. Inst. Metals* **62,** 307–324.

Taylor, G. I. and Elam, C. F. (1923). The distortion of an aluminum crystal during a tensile test. *Proc. R. Soc. Lond.* **A102,** 643–667.

Taylor, G. I. and Elam, C. F. (1925). The plastic extension and fracture of aluminum crystals. *Proc. R. Soc. Lond.* **A108,** 28–51.

von Mises, R. (1928). Mechanik der plastischen Formanderung von Kristallen. *Z. Angew. Meth. Mech.* **8,** 161–185.

APPENDIX A: INTEGRATION ALGORITHM FOR SINGLE CRYSTALLS

The following is a summary of the algorithm given in Maniatty *et al.* (1992). Assume that $\mathbf{F}_n$, $\mathbf{R}^L_n$, $\mathbf{T}_n$ and g_n for the crystal of interest are known at time t_n. Assume also that the macroscopic velocity gradient $\mathbf{L}$ is known at times t_n and t_{n+1}. The value of $\mathbf{F}_{n+1}$ can be determined by integrating

$$\dot{\mathbf{F}} = \mathbf{L}\mathbf{F}$$

using a fourth order Runge–Kutta algorithm. Now, the goal is to find $\mathbf{R}^L_{n+1}$, $\mathbf{T}_{n+1}$ and g_{n+1} at time t_{n+1}. Writing a backward difference expression as an approximation for $\mathbf{F}^p_{n+1}$, solving for $\mathbf{L}^p_{n+1}$ and substituting into eqn (7) gives

$$\mathbf{L}^p_{n+1} = \frac{1}{\Delta t}(\mathbf{I} - \mathbf{F}^p_n \mathbf{F}^{p^{-1}}_{n+1}) = \sum_{\alpha=1}^{N_s} \dot{\gamma}^\alpha_{n+1} \mathbf{P}^\alpha$$

or, rearranging,

$$\mathbf{0} = \sum_{\alpha=1}^{N_s} \dot{\gamma}^\alpha_{n+1} \mathbf{P}^\alpha - \frac{1}{\Delta t}(\mathbf{I} - \mathbf{F}^p_n \mathbf{F}^{p^{-1}}_{n+1}), \tag{A1}$$

where $\mathbf{P}^\alpha$ is known since it is defined on the reference configuration and where

$$\dot{\gamma}^\alpha_{n+1} = \dot{\gamma}(\tau^\alpha_{n+1}, g_{n+1}). \tag{A2}$$

Now, substituting eqn (14) into (8) gives the folowing:

$$\tau^\alpha_{n+1} = [\mu \mathbf{C}^{e^2}_{n+1} - (\mu + \tfrac{3}{2}\lambda - \tfrac{1}{2}\lambda \operatorname{tr} \mathbf{C}^e_{n+1} - \beta)\mathbf{C}^e_{n+1} - \beta \mathbf{C}^e_{n+1} \mathscr{C}[\mathbf{C}^e_{n+1}]] \cdot \mathbf{P}^\alpha, \tag{A3}$$

where

$$\mathbf{C}^e_{n+1} = \mathbf{F}^{*\mathrm{T}}_{n+1} \mathbf{F}^*_{n+1} = \mathbf{F}^{p^{-\mathrm{T}}}_{n+1} \mathbf{F}^{\mathrm{T}}_{n+1} \mathbf{F}_{n+1} \mathbf{F}^{p^{-1}}_{n+1}, \tag{A4}$$

which is obtained using eqn (1). If eqn (A4) is substituted into eqn (A3), and then (A3) into (A2), and finally (A2) into (A1), one large equation for $\mathbf{F}^p_{n+1}$ results. The solution algorithm can now be summarized as follows:

1. Solve eqn. (A1) for $\mathbf{F}^p_{n+1}$ using eqns (A2)–(A4) using a Newton–Raphson type algorithm.
2. Project $\mathbf{F}^p_{n+1}$ onto the space where $\det(\mathbf{F}^p_{n+1}) = 1$, so that $\mathbf{F}^p_{n+1}$ satisfies the constraint in eqn (1).
3. Update g_{n+1} implicitly using

$$g_{n+1} = g_n + \dot{g}_{n+1} \Delta t,$$

   where $\dot{g}_{n+1}$ is defined in eqns (10)–(13).
4. Check for convergence on g_{n+1}. If not converged, go to step 1, otherwise continue.
5. Compute $\mathbf{F}^*_{n+1}$ from $\mathbf{F}^*_{n+1} = \mathbf{F}_{n+1} \mathbf{F}^{p^{-1}}_{n+1}$.
6. Perform the polar decomposition $\mathbf{R}^L_{n+1} \mathbf{U}^e_{n+1} = \mathbf{F}^*_{n+1}$ to obtain $\mathbf{R}^L_{n+1}$.
7. Compute the elastic strain

$$\mathbf{E}^e_{n+1} = \tfrac{1}{2}(\mathbf{F}^{*\mathrm{T}}_{n+1} \mathbf{F}^*_{n+1} - \mathbf{I})$$

   and the stress

$$\hat{\mathbf{T}}_{n+1} = 2\mu \mathbf{E}^e_{n+1} + \lambda(\operatorname{tr} \mathbf{E}^e_{n+1})\mathbf{I} - 2\beta \mathscr{C}[\mathbf{E}^e_{n+1}].$$

8. Compute the Cauchy stress

$$\mathbf{T}_{n+1} = \frac{1}{\det \mathbf{F}^*_{n+1}} \mathbf{F}^*_{n+1} \hat{\mathbf{T}}_{n+1} \mathbf{F}^{*\mathrm{T}}_{n+1}.$$